Physics – Uspekhi **58** (10) 993 – 1001 (2015)

CONFERENCES AND SYMPOSIA

PACS numbers: **75.85.+t**, **76.50.+g**, 78.20.Fm

Dynamic magnetoelectric phenomena with electromagnons in rare-earth borate multiferroics

A A Mukhin, A M Kuzmenko, V Yu Ivanov,
A G Pimenov, A M Shuvaev, V E Dziom

DOI: 10.3367/UFNe.0185.201510l.1089

Contents

Abstract. Electroactive spin excitations (electromagnons), an analog of the low-frequency quasiferromagnetic antiferromagnetic resonance (AFMR) mode in Fe subsystem, are observed in multiferroic rare-earth ferroborates [specifically in $SmFe_3(BO_3)_4$] in the frequency range of 40–150 GHz, which are shown to contribute dominantly to the giant static (quasistatic) magnetodielectric effect and which produce two types of dynamic magnetoelectric effects: (a) giant optical activity, which occurs for the wave vector k parallel to the crystallographic c-axis, $\mathbf{k} \parallel c$, in a transverse magnetic field $\mathbf{H} \parallel a$ and is accompanied by polarization-plane rotation by more than 70 deg mm^{-1} in the resonance, and (b) directional birefringence and dichroism in a transverse magnetic field $\mathbf{H} \parallel b$-axis, which show up in transmission asymmetry between the forward $(\mathbf{k} \parallel c)$ and backward $(\mathbf{k} \parallel -c)$ directions, being equivalent to the sign change of the magnetic field, $H_b \to -H_b$. A theory is developed which explains the observed dynamic magnetoelectric phenomena quantitatively by taking into consideration different symmetries of the tensors of magnetic, magnetoelectric, and dielectric susceptibilities for $\mathbf{H} \parallel a$ and $\mathbf{H} \parallel b$.

Keywords: magnetoelectric phenomena, multiferroics, magnetic excitations, magnetic spectroscopy, antiferromagnetic resonance

A A Mukhin, A M Kuzmenko, V Yu Ivanov Prokhorov General Physics Institute, Russian Academy of Sciences,
ul. Vavilova 38, 119991 Moscow, Russian Federation
E-mail: mukhin@ran.gpi.ru
A G Pimenov, A M Shuvaev, V E Dziom Institute of Solid State Physics, Vienna University of Technology, 1040 Vienna, Austria

Received 20 July 2015
Uspekhi Fizicheskikh Nauk **185** (10) 1089 – 1098 (2015)
DOI: 10.3367/UFNr.0185.201510l.1089
Translated by E G Strel'chenko; edited by A Radzig

1. Introduction

There is increasing recent interest in so-called multiferroics, i.e. materials in which magnetic and ferroelectric order coexist and which are promising for the development of novel functional materials and devices [1–7]. The coupling between the magnetic and electric degrees of freedom in these materials has the consequence that ferroelectrics exhibit new physical properties. The latter can be manipulated by applying an external magnetic or electric field, the propagation of electromagnetic radiation can be controlled, and in ordered magnetic and electrical subsystems a new type of elementary excitations, known as electromagnons, occur, which was first discovered in $TbMnO_3$ and $GdMnO_3$ multiferroics with a cycloidal magnetic structure [8], and later on in several other multiferroics [9–19].

The electromagnon can be defined as an electrically active spin-wave which contributes resonantly to the dielectric constant due to strong spin–lattice interaction with the phonon subsystem. The discovery of electromagnons has stimulated extensive research into various optical (dynamic) magnetoelectric phenomena in multiferroics, such as directional dichroism (i.e. the absorption by the electromagnon is different for forward and backward directions of light propagation through the crystal [20–23]), and a number of other effects [24–26].

A notable recent development is the discovery of a new class of multiferroics comprising the rare-earth ferroborates and alumoborates $RFe_3(BO_3)_4$ and $RAl_3(BO_3)_4$ (where R is the rare-earth element) which exhibit exceptionally strong magnetoelectric effects [27–30]. Unlike manganites, these compounds crystallize in the noncentrosymmetric structure (space group R32 or $P3_121$), so that the polarization in such borates has no relation to the formation of incommensurate cycloidal magnetic structures but rather is induced either within an ordinary collinear antiferromagnetic ordering of Fe^{3+} ions or by an external magnetic field. In ferroborates,

the Fe–Fe interaction determines the Néel temperature (30–40 K). In addition, a key factor is R–Fe exchange, which produces either an easy-plane or an easy-axis magnetic structure, depending on the anisotropy of the rare-earth subsystem. Rare-earth ions also play a key role in the formation of magnetoelectric properties.

As far as the observation of pronounced dynamic magnetoelectric effects is concerned, one of the most attractive systems is the easy-plane $SmFe_3(BO_3)_4$ ferroborate, which was found to exhibit a giant magnetoelectric effect at frequencies up to 1 MHz due to, first, the increase (by $\sim 300\%$) in the dielectric constant with decreasing temperature from the Néel point to 4.2 K and, second, the strong influence of the magnetic field on the compound [31]. Essentially, this effect is due to the contribution to the dielectric constant from the electric susceptibility due to rotation of iron spins in the easy *ab* plane, which arise in the antiferromagnetic state for $T < T_N = 33$ K, where T_N is the Néel temperature, and which is suppressed by the external magnetic field. Obviously, electroactive spin excitations must be present in the interacting Fe and Sm subsystems, which are responsible for the giant contribution to the dielectric constant. Our earlier quasioptical studies in the frequency range of 150–600 GHz (a high-frequency antiferromagnetic resonance of Fe^{3+} ions and electronic transitions in the ground doublet of Sm^{3+} ions) showed that these excitations are essentially of a magnetoactive nature and they contribute only slightly to the dielectric constant [32]. Therefore, the spin excitation most likely responsible for the giant magnetoelectric effect is the low-frequency (quasiferromagnetic) AFMR mode which corresponds to the oscillations of Fe^{3+} spins in the easy basis plane and lies in the frequency range of $\sim 5-10$ GHz at $H = 0$ (but can be shifted to much higher frequencies if magnetic field is present).

This paper presents gigahertz spectroscopy results on single-crystal ferroborate $SmFe_3(BO_3)_4$, which were obtained in the region of such an electroactive AFMR mode and which demonstrate a series of unusual resonant magnetoelectric effects (optical activity and directional dichroism, and birefringence). Some of these results have been published elsewhere [33].

2. Experiment

The transmission spectra $T(\nu)$ and phase shifts were measured in the frequency range $\nu = 40-1000$ GHz at temperatures of 4–300 K in magnetic fields up to 7 T using quasioptical polarization backward wave oscillator (BWO) spectroscopy [34]. In all measurements, the magnetic field was perpendicular to the propagation vector (Vogt geometry). The borate samples were plane-parallel, oriented single-crystal plates with thicknesses of $\approx 1-2$ mm and size of $\approx 5-6$ mm, grown by L N Bezmaternykh and I A Gudim at the L V Kirenskii Institute of Physics, Siberian Branch of the Russian Academy of Sciences, Krasnoyarsk.

3. Results and discussion

3.1 Electroactive nature of the quasiferromagnetic antiferromagnetic resonance mode

In an easy-plane antiferromagnet, even a relatively weak external magnetic field **H** applied in the easy plane aligns the spins perpendicular to its direction, so that the low-frequency quasiferromagnetic AFMR mode is excited by the alternating magnetic field $\mathbf{h} \perp \mathbf{H}$, and must not be excited if the polarization is $\mathbf{h} \parallel \mathbf{H}$.

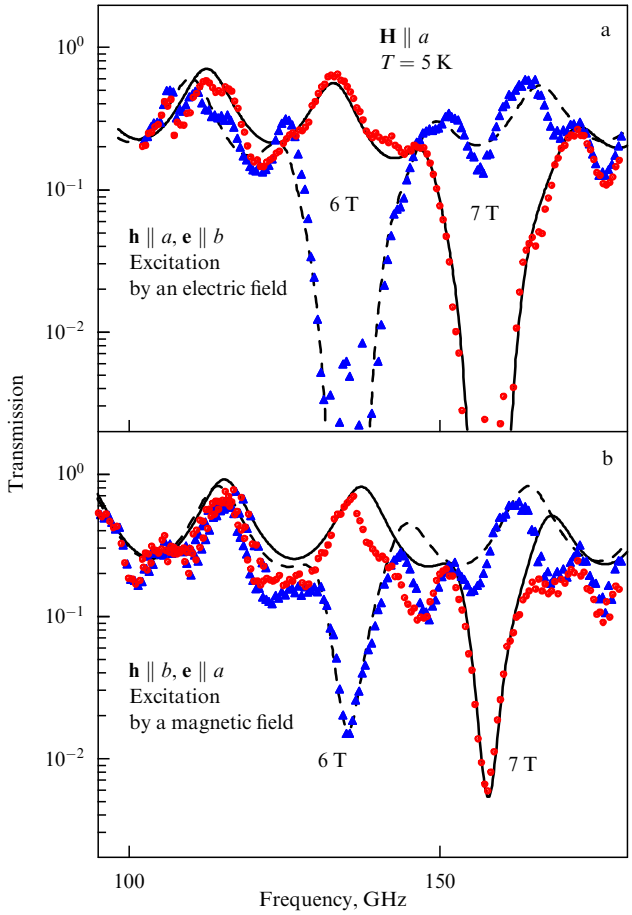

Figure 1. Examples of transmission spectra of a 1.756-mm thick *c*-cut $SmFe_3(BO_3)_4$ plate in the frequency range of an electroactive AFMR mode (electromagnon) in external magnetic field $\mathbf{H} \parallel a$ for polarization $\mathbf{h} \parallel a$, $\mathbf{e} \parallel b$, when the mode is excited by an electric field (a) and for polarization $\mathbf{h} \parallel b$, $\mathbf{e} \parallel a$, when the excitation is provided by a magnetic field (b). Symbols — experiment, and lines — simulation.

Shown in Fig. 1 are the examples of transmission spectra of a *c*-cut plane-parallel sample of $SmFe_3(BO_3)_4$ in the frequency range of the low-frequency AFMR mode in external magnetic field $\mathbf{H} \parallel a$ for two incident radiation polarizations. It is seen that not only under classical excitation conditions, $\mathbf{h} \perp \mathbf{H}$ (Fig. 1b), but also for $\mathbf{h} \parallel \mathbf{H}$ (Fig. 1a), i.e., for the polarization $\mathbf{h} \parallel a$ forbidden for excitation by ac magnetic field, the AFMR mode is clearly detected against the background of transmission oscillations due to the interferences in a plane-parallel sample. This is an indication that the excitation in this case is caused by the electric rather than magnetic component, $\mathbf{e} \parallel b$, of the electromagnetic field, directly pointing to the electroactive nature of the AFMR mode (electromagnon).

Simulation results obtained for the transmission spectra on the basis of Fresnel formulas and including the resonant contribution from the AFMR mode to the magnetic permeability and dielectric constant are shown in Fig. 1 by solid and dashed lines. The extracted magnetic field variations of the electromagnon resonance frequency and of the electromagnon contribution to the dielectric constant $\Delta\varepsilon_b$ and magnetic permeability $\Delta\mu_b$ (Fig. 2)

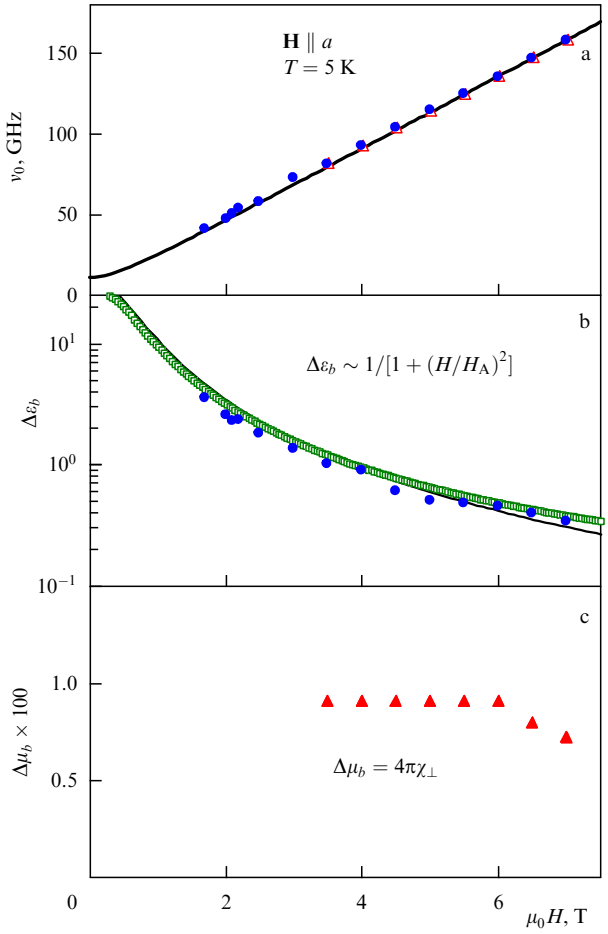

Figure 2. (a) Resonant frequency of the electromagnon, (b) electromagnon contribution to the dielectric constant $\Delta\varepsilon_b$, and (c) electromagnon contribution to the magnetic permeability $\Delta\mu_b$ as a function of external magnetic field $\mathbf{H} \| a$. Circles and triangles — spectroscopic data, squares — static dielectric constant, and lines — simulation results.

correspond well to the available statical data and to simulation (see below).

3.2 Theory of dynamic magnetoelectric properties of ferroborates

Before proceeding to the remaining experimental results on $SmFe_3(BO_3)_4$, let us examine the major aspects of the resonance magnetic, dielectric, and magnetoelectric properties of ferroborates. Let us begin with the thermodynamic potential of a system as a function of the ferromagnetic ($\mathbf{m}$) and antiferromagnetic ($\mathbf{l}$) ordering vectors of the Fe subsystem, the electric polarization $\mathbf{P}$, and external magnetic ($\mathbf{H}$) and electric ($\mathbf{E}$) fields:

$$\Phi(\mathbf{m},\mathbf{l},\mathbf{P},\mathbf{H},\mathbf{E}) = \Phi_{\rm m}(\mathbf{m},\mathbf{l},\mathbf{H}) + \Phi_{\rm me}(\mathbf{m},\mathbf{l},\mathbf{P}) + \Phi_{\rm e}(\mathbf{P},\mathbf{E})\,, \quad (1)$$

where $\Phi_{\rm m}(\mathbf{m},\mathbf{l},\mathbf{H})$, $\Phi_{\rm me}(\mathbf{m},\mathbf{l},\mathbf{P})$, and $\Phi_{\rm e}(\mathbf{P},\mathbf{E})$ are the magnetic, magnetoelectric, and electrical parts, respectively. The magnetic part of the thermodynamic potential is given by the expression

$$\Phi_{\rm m}(\mathbf{m},\mathbf{l},\mathbf{H}) = \frac{1}{2}\,A\mathbf{m}^2 - M_0\mathbf{m}\mathbf{H} + \Phi_{\rm A}(\mathbf{l})\,, \quad (2)$$

where the first two terms are the exchange and Zeeman energies, respectively, and the last term is the anisotropy energy

$$\Phi_{\rm A}(\mathbf{l}) = \frac{1}{2}\,K_{\rm eff} l_z^2 + \frac{1}{12}\,K_6\left[(l_x + {\rm i}l_y)^6 + (l_x - {\rm i}l_y)^6\right] - \frac{1}{2}\,K_{1u}(l_x^2 - l_y^2) - K_{2u} l_x l_y\,,$$

which includes the effective uniaxial anisotropy energy and the anisotropy energy in the basis plane, the former of which stabilizes the basis ab ($K_{\rm eff} > 0$) plane, and the latter is determined by the hexagonal crystallographic anisotropy (K_6) and by the magnetoelastic anisotropy $K_{1u} \sim \sigma_{xx} - \sigma_{yy}$, $K_{2u} \sim \sigma_{xy}$ induced by internal stresses (compression and expansion, $\sigma_{xx} - \sigma_{yy}$, and shear, σ_{xy}) in the crystal's ab plane. The x, y, z axes coincide with crystallographic a, b, c axes. The magnetoelectric and electric parts of the potential, which are relevant to the resonant phenomena under study, have the form [28, 31]

$$\Phi_{\rm me}(\mathbf{m},\mathbf{l},\mathbf{P}) = -c_2 P_x(l_x^2 - l_y^2) + 2c_2 P_y l_x l_y + \ldots \quad (3)$$

$$\Phi_{\rm e}(\mathbf{P},\mathbf{E}) = \frac{P_x^2 + P_y^2}{2\chi_\perp^{\rm e}} + \frac{P_z^2}{2\chi_\|^{\rm e}} - \mathbf{P}\mathbf{E}\,, \quad (4)$$

where $\chi_\|^{\rm e}$ and $\chi_\perp^{\rm e}$ are the components of the lattice electric (dielectric) susceptibility parallel and perpendicular to the third-order c-axis. The explicit contribution of the rare-earth (Sm) subsystem to the thermodynamic potential (1)–(3) is not considered here, but it is assumed that the system renormalizes the corresponding parameters (A, $K_{\rm eff}$, c_2, ...) due to the $R-$Fe exchange interaction.

Minimizing the thermodynamic potential Φ (1) with respect to the polarization $\mathbf{P}$ gives a direct relation between the polarization and the orientation of the Fe spins (i.e., vector $\mathbf{l}$):

$$\begin{aligned} P_x &= P_0(l_x^2 - l_y^2) + \chi_\perp^{\rm e} E_x\,,\\ P_y &= -P_0 2 l_x l_y + \chi_\perp^{\rm e} E_y\,,\\ P_z &= \chi_\|^{\rm e} E_z\,, \end{aligned} \quad (5)$$

where $P_0 = c_2\chi_\perp^{\rm e}$ determines the maximum polarization induced in the basis plane by the antiferromagnetically ordered Fe subsystem. To describe the dynamics of the magnetic subsystem, i.e., of the variables $\mathbf{m}$ and $\mathbf{l}$, we take advantage [after eliminating $\mathbf{P}$ from Φ in formula (1)] of the Landau–Lifshitz equations

$$\begin{aligned} \frac{M_0}{\gamma}\,\dot{\mathbf{m}} &= \mathbf{m}\times\mathbf{\Phi}_{\mathbf{m}} + \mathbf{l}\times\mathbf{\Phi}_{\mathbf{l}}\,,\\ \frac{M_0}{\gamma}\,\dot{\mathbf{l}} &= \mathbf{m}\times\mathbf{\Phi}_{\mathbf{l}} + \mathbf{l}\times\mathbf{\Phi}_{\mathbf{m}}\,, \end{aligned} \quad (6)$$

where $\mathbf{\Phi}_{\mathbf{m}} = \partial\Phi/\partial\mathbf{m}$, $\mathbf{\Phi}_{\mathbf{l}} = \partial\Phi/\partial\mathbf{l}$, and $\gamma = g_{\rm Fe}\,\mu_{\rm B}/\hbar$ is the gyromagnetic ratio for the Fe^{3+} ions. Solving these equations of motion in the linear approximation and for small deviations of $\Delta\mathbf{m}$ and $\Delta\mathbf{l}$ from the equilibrium state $\mathbf{l}_0 \perp \mathbf{H}$ and $\mathbf{m}_0 \| \mathbf{H}$ (which is stabilized by an external magnetic field exceeding the anisotropy field in the basis plane), we obtain the magnetic and electric responses to the alternating electromagnetic field $\mathbf{e}$ and $\mathbf{h}$:

$$\begin{aligned} \Delta\mathbf{m} &= \hat{\chi}^{\rm m}\mathbf{h} + \hat{\chi}^{\rm me}\mathbf{e}\,,\\ \Delta\mathbf{p} &= \hat{\chi}^{\rm em}\mathbf{h} + \hat{\chi}^{\rm e}\mathbf{e}\,, \end{aligned} \quad (7)$$

which are determined by the magnetic, $\hat{\chi}^{\rm m}$, magnetoelectric, $\hat{\chi}^{\rm me}$ and $\hat{\chi}^{\rm em}$, and dielectric $\hat{\chi}^{\rm e}$ susceptibilities. The form of the

corresponding susceptibility matrices depends on the orientation of the applied magnetic field in the *ab* plane and also on the system's ground state in the field.

For $\mathbf{H} \parallel a$ ($\mathbf{l}_0 \parallel b, \mathbf{m}_0 \parallel \mathbf{P}_0 \parallel a$), we have

$$\hat{\chi}^{\mathrm{m}}(\omega) = \begin{pmatrix} \chi^{\mathrm{m}}_{xx} & 0 & 0 \\ 0 & \chi^{\mathrm{m}}_{yy} & \chi^{\mathrm{m}}_{yz} \\ 0 & \chi^{\mathrm{m}}_{zy} & \chi^{\mathrm{m}}_{zz} \end{pmatrix}, \quad \hat{\chi}^{\mathrm{me}}(\omega) = \begin{pmatrix} \chi^{\mathrm{me}}_{xx} & 0 & 0 \\ 0 & \chi^{\mathrm{me}}_{yy} & 0 \\ 0 & \chi^{\mathrm{me}}_{zy} & 0 \end{pmatrix},$$

$$\hat{\chi}^{\mathrm{em}}(\omega) = \begin{pmatrix} \chi^{\mathrm{em}}_{xx} & 0 & 0 \\ 0 & \chi^{\mathrm{em}}_{yy} & \chi^{\mathrm{em}}_{yz} \\ 0 & 0 & 0 \end{pmatrix}, \quad \hat{\chi}^{\mathrm{e}}(\omega) = \begin{pmatrix} \chi^{\mathrm{e}}_{xx} & 0 & 0 \\ 0 & \chi^{\mathrm{e}}_{yy} & 0 \\ 0 & 0 & \chi^{\mathrm{e}}_{zz} \end{pmatrix}, \tag{8}$$

where the matrix components are expressed as follows:

$$\begin{aligned} &\chi^{\mathrm{m}}_{xx} = \chi_{\perp} L_{\mathrm{AF}}(\omega)\,, \quad \chi^{\mathrm{m}}_{zz} = \chi_{\perp} L_{\mathrm{F}}(\omega)\,, \quad \chi^{\mathrm{m}}_{yy} = \rho^2 \chi_{\perp} L_{\mathrm{F}}(\omega)\,, \\ &\chi^{\mathrm{m}}_{zy} = -\chi^{\mathrm{m}}_{yz} = -\frac{\mathrm{i}\omega}{\omega_{\mathrm{F}}}\, \rho \chi_{\perp} L_{\mathrm{F}}(\omega)\,, \\ &\chi^{\mathrm{e}}_{yy} = \chi^{\mathrm{e}}_{\perp} + \chi^{\mathrm{e}}_{\mathrm{rot}} L_{\mathrm{F}}(\omega)\,, \quad \chi^{\mathrm{e}}_{xx,\,zz} = \chi^{\mathrm{e}}_{\perp,\,\parallel}\,, \\ &\chi^{\mathrm{me}}_{xx} = \chi^{\mathrm{em}}_{xx} \approx 0\,, \quad \chi^{\mathrm{me}}_{yy} = \chi^{\mathrm{em}}_{yy} = \rho\eta \sqrt{\chi_{\perp}\chi^{\mathrm{e}}_{\mathrm{rot}}}\, L_{\mathrm{F}}(\omega)\,, \\ &\chi^{\mathrm{me}}_{zy} = -\chi^{\mathrm{em}}_{yz} = \frac{\mathrm{i}\omega}{\omega_{\mathrm{F}}}\, \eta \sqrt{\chi_{\perp}\chi^{\mathrm{e}}_{\mathrm{rot}}}\, L_{\mathrm{F}}(\omega)\,. \end{aligned} \tag{9}$$

Here, $\chi_{\perp} = M_0^2/A \equiv M_0/2H_{\mathrm{E}}$ is the transverse susceptibility of the Fe subsystem; M_0 and H_{E} are the magnetization of the antiferromagnetic Fe sublattices and the field of the isotropic Fe–Fe exchange, respectively; $\chi^{\mathrm{e}}_{\mathrm{rot}}(H) = \chi^{\mathrm{e}}_{0\,\mathrm{rot}}/(1 + H^2/H^2_{ab})$ is the electric susceptibility due to the Fe spin rotation in the basis plane, determined by the magnetoelectric interaction and the external magnetic field, with $\chi^{\mathrm{e}}_{0\,\mathrm{rot}} = (2P_0)^2/K'_{\mathrm{A}}$, and $H^2_{ab} = 2H'_{\mathrm{A}}H_{\mathrm{E}}$ is the characteristic field determining the rotation/oscillation of spins in the basis plane, and

$$K'_{\mathrm{A}} = H'_{\mathrm{A}} M_0 = \left.\frac{\partial^2 \Phi_{\mathrm{A}}}{\partial \varphi^2}\right|_{\varphi = \pm\pi/2}$$

is the energy of the effective anisotropy in this plane for the geometry $\mathbf{l}_0 \parallel b$ ($\varphi = \pi/2$). The functions $L_{\mathrm{F,\,AF}}(\omega) = \omega^2_{\mathrm{F,\,AF}}/(\omega^2_{\mathrm{F,\,AF}} - \omega^2 + \mathrm{i}\omega\Delta\omega_{\mathrm{F,\,AF}})$ determine the frequency dispersion of the electrodynamic response in the vicinity of the frequencies $\omega^2_{\mathrm{F}} = \gamma^2(H^2 + H^2_{ab})$ of the quasiferromagnetic mode due to the oscillations of $\mathbf{l}$ in the basis plane, and the frequencies $\omega^2_{\mathrm{AF}} = \gamma^2 2H_{\mathrm{A}}H_{\mathrm{E}}$ of the quasiantiferromagnetic mode due to the deviation of $\mathbf{l}$ from the plane ($H_{\mathrm{A}} = K_{\mathrm{A}}/M_0$ is the anisotropy field), and $\Delta\omega_{\mathrm{F,\,AF}}$ is the line width of the modes. The quantity $\rho = H/(H^2 + H^2_{ab})^{1/2}$ accounting for the change in the antiferromagnetic structure in magnetic field becomes equal to ± 1 in a field above $H_{ab} \sim 5$–10 kOe. The factor $\eta = (V^+ - V^-)/(V^+ + V^-)$ accounts for the possibility that the ferroborate contains opposite-chirality structural twins that make opposite contributions to the electric polarization and have a concentration (volume) $V^{\pm}$.

For $\mathbf{H} \parallel b$, the ground state changes its symmetry ($\mathbf{l}_0 \parallel a \parallel -\mathbf{P}_0$, $\mathbf{m}_0 \parallel b$), thus changing the symmetry of the electrodynamic response. Both AFMR modes then turn out, strictly speaking, to be coupled. However, in magnetic fields that are not too high (up to 7 T), the mode frequency ω_{F} in $SmFe_3(BO_3)_4$ remains considerably smaller than ω_{AF} (~ 320 GHz [32]), allowing their mixing to be neglected. In this case, the dynamic magnetic, magnetoelectric, and dielectric susceptibilities are given for the frequencies of interest (i.e., for those close to the quasiferromagnetic mode) by

$$\hat{\chi}^{\mathrm{m}}(\omega) = \begin{pmatrix} \chi^{\mathrm{m}}_{xx} & 0 & \chi^{\mathrm{m}}_{xz} \\ 0 & \chi^{\mathrm{m}}_{yy} & 0 \\ \chi^{\mathrm{m}}_{zx} & 0 & \chi^{\mathrm{m}}_{zz} \end{pmatrix}, \quad \hat{\chi}^{\mathrm{me}}(\omega) = \begin{pmatrix} 0 & \chi^{\mathrm{me}}_{xy} & 0 \\ 0 & 0 & 0 \\ 0 & \chi^{\mathrm{me}}_{zy} & 0 \end{pmatrix},$$

$$\hat{\chi}^{\mathrm{em}}(\omega) = \begin{pmatrix} 0 & 0 & 0 \\ \chi^{\mathrm{em}}_{yx} & 0 & \chi^{\mathrm{em}}_{yz} \\ 0 & 0 & 0 \end{pmatrix}, \quad \hat{\chi}^{\mathrm{e}}(\omega) = \begin{pmatrix} \chi^{\mathrm{e}}_{xx} & 0 & 0 \\ 0 & \chi^{\mathrm{e}}_{yy} & 0 \\ 0 & 0 & \chi^{\mathrm{e}}_{zz} \end{pmatrix}, \tag{10}$$

where

$$\begin{aligned} &\chi^{\mathrm{m}}_{xx} \approx \chi^{\mathrm{m}}_{zz} \approx \chi_{\perp} L_{\mathrm{F}}(\omega)\,, \quad \chi^{\mathrm{m}}_{yy} \approx \chi_{\perp} L_{\mathrm{AF}}(\omega) \approx \chi_{\perp}\,, \\ &\chi^{\mathrm{m}}_{xz} \approx -\chi^{\mathrm{m}}_{zx} \approx \frac{\mathrm{i}\omega}{\omega_{\mathrm{F}}}\, \rho \chi_{\perp} L_{\mathrm{F}}(\omega)\,, \\ &\chi^{\mathrm{e}}_{xx} \approx \chi^{\mathrm{e}}_{\perp}\,, \quad \chi^{\mathrm{e}}_{yy} \approx \chi^{\mathrm{e}}_{\perp} + \chi^{\mathrm{e}}_{\mathrm{rot}} L_{\mathrm{F}}(\omega)\,, \quad \chi^{\mathrm{e}}_{zz} \approx \chi^{\mathrm{e}}_{\parallel}\,, \\ &\chi^{\mathrm{me}}_{xy} \approx \chi^{\mathrm{em}}_{yx} \approx \rho\eta \sqrt{\chi_{\perp}\chi^{\mathrm{e}}_{\mathrm{rot}}}\, L_{\mathrm{F}}(\omega)\,, \\ &\chi^{\mathrm{me}}_{zy} \approx -\chi^{\mathrm{em}}_{yz} \approx -\frac{\mathrm{i}\omega}{\omega_{\mathrm{F}}}\, \eta \sqrt{\chi_{\perp}\chi^{\mathrm{e}}_{\mathrm{rot}}}\, L_{\mathrm{F}}(\omega)\,. \end{aligned} \tag{11}$$

In deriving the magnetoelectric responses (8) and (10), it was assumed that the resonance frequencies of the rare-earth (Sm) ions, as determined by the splitting of their ground doublet by the exchange R–Fe interaction, lie considerably higher than the AFMR frequencies of the Fe subsystem. This condition is fully satisfied for the low-frequency quasiferromagnetic mode ω_{F}, in the vicinity of which we study magnetoelectric effects. As for the high-frequency quasiantiferromagnetic mode ω_{AF}, its frequency is comparable to that of the Sm modes, and their interaction cannot, therefore, be neglected [32]. However, the dynamic magnetoelectric effects at these frequencies are expected to be smaller — because they are caused by higher-frequency (i.e., harder) spin oscillations — and indeed have not been observed yet. Thus, in general, the electrodynamic response contains additional, symmetry-allowed contributions, which are omitted in Eqns (8) and (9) for simplicity.

Let us discuss how the dynamic magnetoelectric effects manifest themselves in gigahertz quasioptical spectra of $SmFe_3(BO_3)_4$.

3.3 Giant optical activity in the vicinity of an electromagnon ($\mathbf{H} \parallel a$)

For a magnetic field parallel to the crystallographic *a*-axis, $\mathbf{H} \parallel a$, and assuming the radiation propagation along the *c*-axis, ($\mathbf{k} \parallel c$), the electroactive quasiferromagnetic mode is excited either by the radiation magnetic component h_y (through χ^{m}_{yy}) or by the ac electric component (through χ^{e}_{yy}), both of which are orthogonal to the static electric polarization $\mathbf{P}_0$ and the magnetization $\mathbf{m}_0$, $\mathbf{P}_0 \parallel \mathbf{m}_0 \parallel a(x)$. Note that, as seen from Fig. 2, the magnetic contribution $\Delta\mu_b = 4\pi\chi_{\perp}$ remains unchanged upon changing the field, while the electric contribution $\Delta\varepsilon_b = 4\pi\chi^{\mathrm{e}}_{\mathrm{rot}} = 4\pi\chi^{\mathrm{e}}_{0\,\mathrm{rot}}/(1 + H^2/H^2_{ab})$ decreases with increasing H in full agreement with theory. The decrease in the last contribution is due to enhancing the field-induced anisotropy in the basis plane, which hampers the rotation (oscillations) of the iron spins in

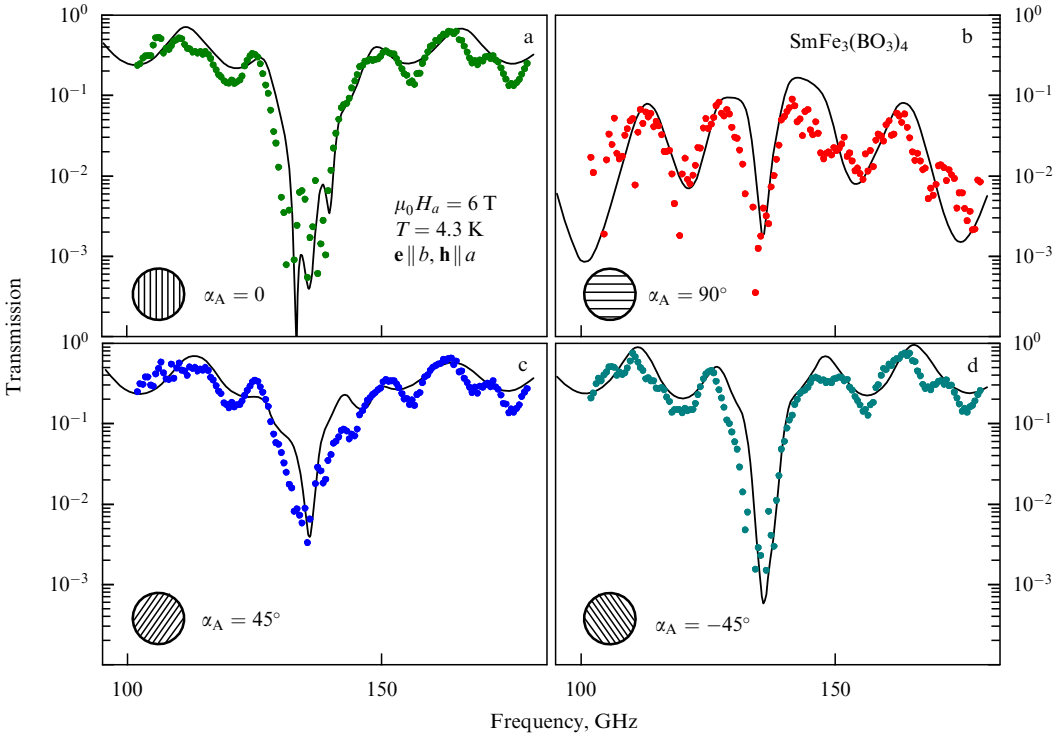

Figure 3. Optical activity in $SmFe_3(BO_3)_4$ in the vicinity of the electromagnon mode. Frequency transmission spectra of a plane-parallel plate at $\mu_0 H_a = 6$ T for different orientations α_A of the analyzer with respect to the polarizer, which sets the polarization of the incident radiation $\mathbf{e} \parallel b$, $\mathbf{h} \parallel a$: (a) parallel, (b) crossed, and (c, d) at angles $\pm 45°$. Symbols — experiment, and lines — simulation.

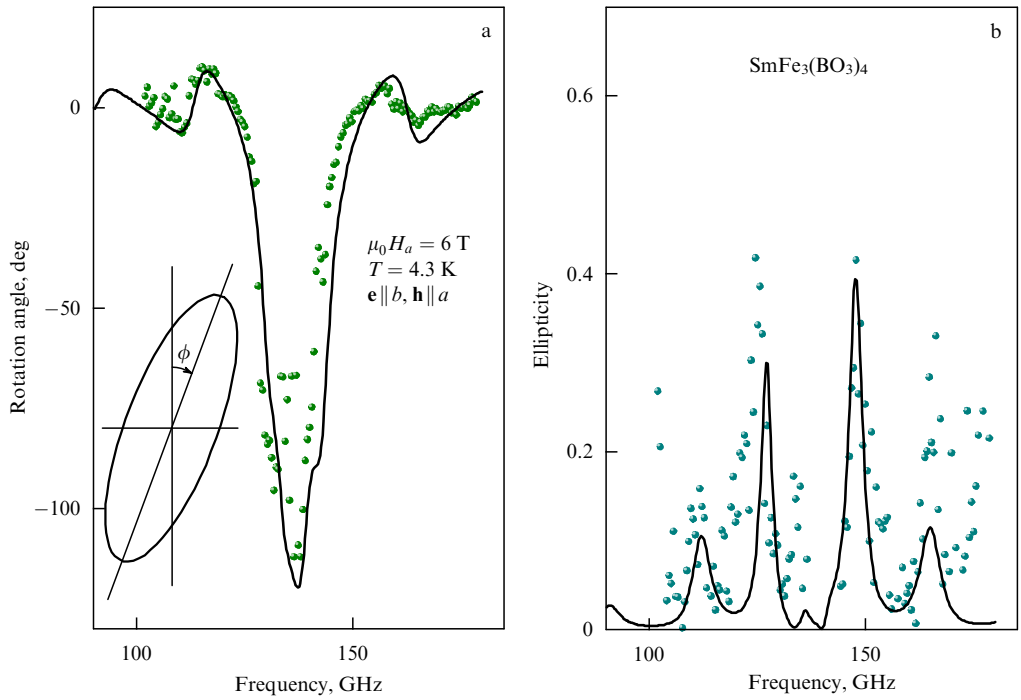

Figure 4. (a) Spectrum of the polarization rotation angle, and (b) the ellipticity of radiation close to the electromagnon frequency for incident radiation polarization $\mathbf{e} \parallel b$, $\mathbf{h} \parallel a$ in the magnetic field $\mu_0 H_a = 6$ T. Symbols — experiment, and lines — simulation.

electric field and which also causes the resonant frequency $\omega_F = \gamma(H^2 + H_{ab}^2)^{1/2}$ to increase (Fig. 2a).

The dynamic magnetoelectric susceptibility $\hat{\chi}^{me}$, $\hat{\chi}^{em}$, or, more specifically, the presence of the diagonal components $\chi_{yy}^{me} = \chi_{yy}^{em} = \rho\eta\sqrt{\chi_\perp \chi_{rot}^e}\, L_F(\omega)$, is another fundamental factor determining the electrodynamics of the system. As linearly polarized wave propagates in a crystal, these components have the effect of entangling the originally orthogonal **e** and **h** components, causing the polarization plane to rotate and changing the ellipticity of the wave. The solution of Maxwell's equations shows that in this case the eigenmodes in a magnetoelectric crystal are two elliptically polarized modes

traveling along the axis $c \| z$, for which the refractive indices and the field component ratios are given by

$$(n_z^{\pm})^2 = \varepsilon_{xx}\,\tilde{\mu}_{yy} + \tilde{\varepsilon}_{yy}\mu_{xx} \pm \sqrt{(\varepsilon_{xx}\,\tilde{\mu}_{yy} - \tilde{\varepsilon}_{yy}\,\mu_{xx})^2 + \varepsilon_{xx}\,\mu_{xx}\tilde{\alpha}_{yy}^2}\,,$$
$$\left(\frac{E_y}{E_x}\right)^{\pm} = \frac{\tilde{\alpha}_{yy}\varepsilon_{xx}\,\mu_{xx}}{n_z^{\pm}(n_z^{\pm\,2} - \tilde{\varepsilon}_{yy}\,\mu_{xx})}\,, \qquad (12)$$

where

$$\hat{\mu} = \hat{1} + 4\pi\hat{\chi}^{\,\mathrm{m}}\,, \quad \hat{\varepsilon} = \hat{1} + 4\pi\hat{\chi}^{\,\mathrm{e}}\,, \quad \hat{\alpha}^{\,\mathrm{me,em}} = 4\pi\hat{\chi}^{\,\mathrm{me,em}}\,,$$
$$\tilde{\mu}_{yy} = \mu_{yy} - \frac{\mu_{zy}\,\mu_{yz}}{\mu_{zz}}\,, \quad \tilde{\varepsilon}_{yy} = \varepsilon_{yy} - \frac{\alpha_{zy}^{\mathrm{me}}\alpha_{yz}^{\mathrm{em}}}{\mu_{zz}}\,, \quad \tilde{\alpha}_{yy} = \alpha_{yy} - \frac{\mu_{zy}\alpha_{yz}^{\mathrm{em}}}{\mu_{zz}}\,.$$

The optical activity of $SmFe_3(BO_3)_4$ was studied by measuring the transmission spectra in the vicinity of the electromagnon mode for different orientations α_A of the analyzer with respect to the polarizer. Figure 3 gives examples of such spectra for the incident polarization $\mathbf{e} \| b$, $\mathbf{h} \| a$ in the magnetic field $\mu_0 H_a = 6$ T. Note the qualitative differences between $\alpha_A = \pm 45°$ spectra, which should be equivalent in the case of nonrotating polarization, and note also the strong transmission for the crossed analyzer and polarizer ($\alpha_A = 90°$), which indicates a considerable rotation of the polarization plane. To characterize the radiation at the output from the sample, we took advantage of the transmission spectra obtained for different α_A, and calculated the angle Θ of the polarization-plane rotation and the ellipticity ρ using the expressions

$$\tan(2\Theta) = \frac{1}{2}\,\frac{T_{45} - T_{-45}}{T_0 + T_{90}}\,,$$
$$\rho = \left(\frac{E_{\min}}{E_{\max}}\right)^2 = \left[1 - \frac{1}{16}\,\frac{(T_{45} - T_{-45})^2}{T_0 T_{90}}\right]^{1/2}, \qquad (13)$$

where T_0, T_{45}, T_{-45}, T_{90} are the transmission coefficients at $\alpha_A = 0, \pm 45°$, and $90°$, respectively. Shown in Fig. 4 are the angle spectra of a polarization-plane rotation and of ellipticity calculated in this way in the frequency range close to the electromagnon and for the incident radiation polarization $\mathbf{e} \| b$, $\mathbf{h} \| a$. Note a very large polarization-plane rotation angle of more than 120° for the sample thickness of only ≈ 1.7 mm. It is also to be emphasized that this rotation is purely magnetoelectric in nature and the external transverse magnetic field is basically needed only to increase the electromagnon frequency to a conveniently measurable range. The observed optical activity is fundamentally different from the ordinary Faraday rotation which is determined solely by the off-diagonal components of the magnetic permeability or dielectric constant and manifests itself only at $\mathbf{k} \| \mathbf{H}$.

To understand the observed phenomena in more detail, simulations of transmission spectra accounting for polarization plane rotation were performed by calculating the transmission matrices (Jones matrices for E_x, E_y, and Berreman matrices [35] for E_x, E_y, H_x, H_y) using Maxwell's equations, including radiation interference in multiple reflections from surfaces in a plane-parallel sample (normal incidence; see also Ref. [33]). The calculations used relations (8) as constitutive equations. The calculated results, shown as solid lines in Figs 3 and 4, are in good agreement with the experimental data.

The fitting parameters involved were the lattice transverse dielectric constant $\varepsilon_\perp = 4\pi\chi_\perp^{\mathrm{e}} = 13.7 - 0.04\mathrm{i}$, the magnetoelectric contribution to the static dielectric constant $\Delta\varepsilon_{0\,\mathrm{rot}} = 4\pi\chi_{0\,\mathrm{rot}}^{\mathrm{e}} \approx 40$, the characteristic field $H_{ab} \approx 5$ kOe determining the rotation/oscillations of spins in the basis plane, the contribution to the magnetic permeability $\Delta\mu_\perp = 4\pi\chi_\perp \approx 8.5 \times 10^{-3}$, the linewidth of the quasiferromagnetic mode, $\Delta\nu_{\mathrm{F}} = \Delta\omega_{\mathrm{F}}/2\pi \approx 4.5$ GHz, and the factor $\eta \approx 0.59$ accounting for the presence of inversion twins in the crystal and giving their volume ratio in our sample, $V^-/V^+ \sim 20/80$. When the twin volumes are equal, $V^+ = V^-$ ($\eta = 0$), the yy-component of the magnetoelectric susceptibility is zero and the polarization plane does not rotate, but the mode still continues to be excited by the electric field. Note that due to the weak repulsive interaction with the above-lying Sm mode, the effective gyromagnetic ratio γ of the Fe subsystem is about 20% less than its classical value for magnetic ions with a g-factor of ~ 2.

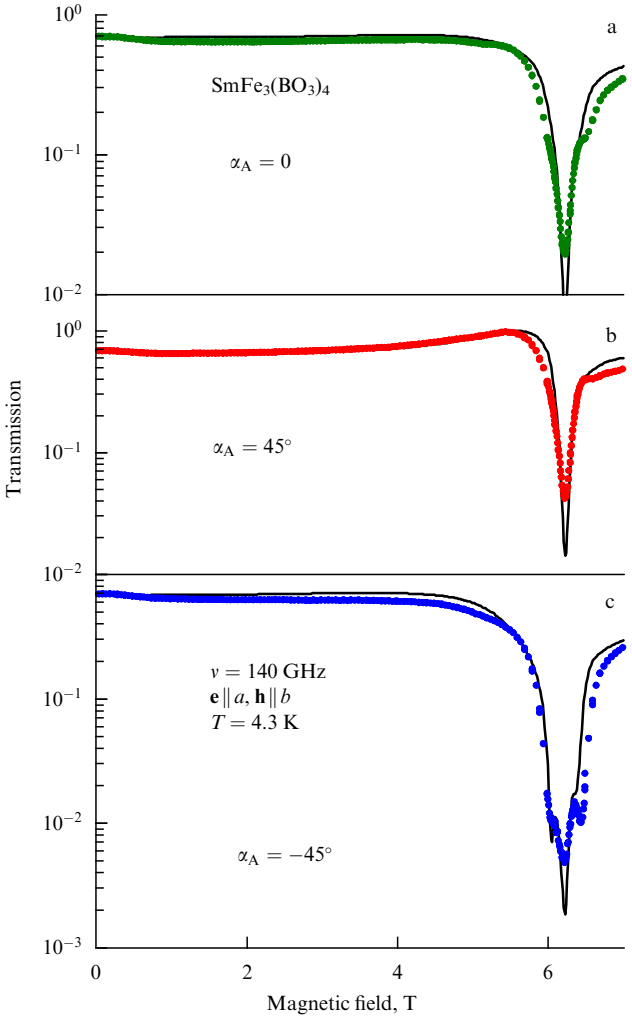

Figure 5. Optical activity of $SmFe_3(BO_3)_4$ in the vicinity of the electromagnon mode. Field transmission spectra at $\nu = 140$ GHz for different analyzer orientations α_A relative to the polarizer which sets the incident polarization $\mathbf{e} \| a$, $\mathbf{h} \| b$: (a) parallel, and (b, c) at angles $\pm 45°$. Symbols — experiment, and lines — simulation.

Optical activity in the vicinity of the electromagnon mode in $SmFe_3(BO_3)_4$ was also observed in the transmission spectra measured at a fixed frequency. Figure 5 depicts such spectra at $\nu = 140$ GHz for different analyzer orientations α_A with respect to the polarizer that sets the incident radiation polarization $\mathbf{e} \| a$, $\mathbf{h} \| b$. Similarly to the frequency spectra, the

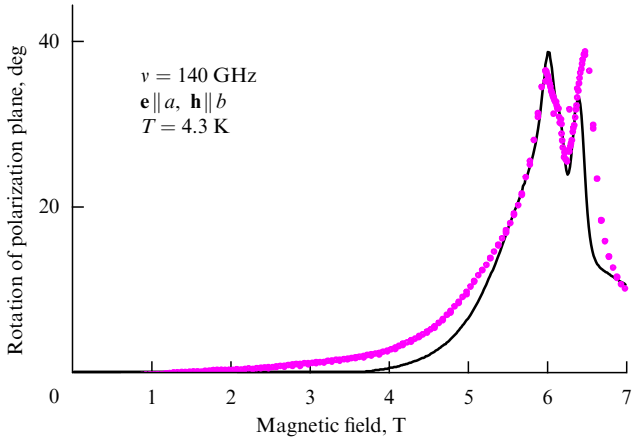

Figure 6. Magnetic field dependence of the polarization rotation angle close to the electromagnon at $\nu = 140$ GHz. Symbols — experiment, and lines — simulation.

line shape and the intensity are observed to vary significantly with the analyzer orientation α_A, indicative of the rotation of the polarization plane, as shown in Fig. 6. The smaller angle of a polarization plane rotation compared with that in Fig. 4a is due to the different incident radiation polarization. Simulations of the transmission and polarization rotation with the parameters obtained earlier agree well with experiment, indicating the suitability of the proposed approach to describe the magnetoelectric phenomena.

3.4 Directional dichroism and birefringence in the vicinity of an electromagnon ($\mathbf{H} \| b$)

In a magnetic field applied parallel to the crystallographic b-axis, $\mathbf{H} \| b$, the symmetry of the ground state of the system becomes different from that in the $\mathbf{H} \| a$ geometry. In this case, the magnetization and polarization are not collinear and produce in the system a nonzero toroidal moment, $\mathbf{T} \propto \mathbf{P} \times \mathbf{m}$, due to which an asymmetry between the forward and backward propagation directions arises [20–23]. Solving Maxwell's equations for the actual symmetry of the electrodynamic response (10) shows that in this case (for $\mathbf{k} \| c$) two linearly polarized modes are eigenmodes.

The first mode, with polarization $\mathbf{h} \| y \| \mathbf{H}$, $\mathbf{e} \| x \| \mathbf{P}$, has the refractive index

$$n_z^{\pm} = \pm\sqrt{\varepsilon_{xx}\,\mu_{yy}}\,, \tag{14}$$

which produces no resonance in the electromagnon frequency range and whose magnitude does not depend on the propagation direction according to the signs $\pm$.

For the second mode, with polarization $\mathbf{h} \| x \perp \mathbf{H}$, $\mathbf{e} \| y \perp \mathbf{P}$, the refractive index takes the form

$$n_z^{\pm} = \pm\sqrt{\tilde{\varepsilon}_{yy}\,\tilde{\mu}_{xx}} + \tilde{\alpha}_{xy} \equiv \pm n_{z0} + \tilde{\alpha}_{xy} \tag{15}$$

(where $\tilde{\mu}_{xx} = \mu_{xx} - \mu_{zx}\,\mu_{xz}/\mu_{zz}$, $\tilde{\varepsilon}_{yy} = \varepsilon_{yy} - \alpha_{zy}^{\mathrm{me}}\alpha_{yz}^{\mathrm{em}}/\mu_{zz}$, $\tilde{\alpha}_{xy} = \alpha_{xy} - \mu_{xz}\alpha_{zy}^{\mathrm{me}}/\mu_{zz}$), giving rise to both magnetically and electrically excited resonance and to the dependence of the refractive index on the propagation direction.

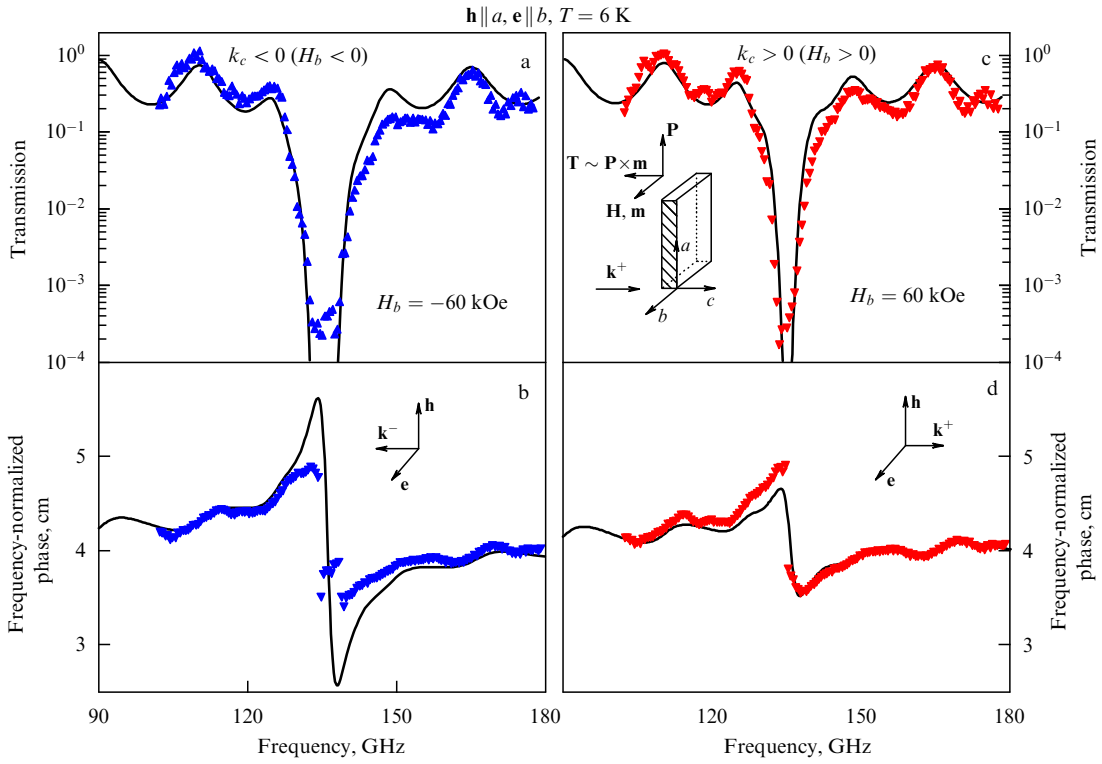

Figure 7. Absorption and refraction asymmetry in $SmFe_3(BO_3)_4$ close to the electromagnon frequency for the forward and backward radiation propagation directions (directional dichroism and birefringence). Transmission spectra (a, c) and frequency-normalized phase spectra (b, d) for propagation with polarization $\mathbf{h} \| a$, $\mathbf{e} \| b$ in the forward ($k_c > 0$) (c, d) and backward ($k_c < 0$) (a, b) directions (the latter amounting to changing the sign of the b-aligned 60-kOe magnetic field). The inset shows the experimental geometry, i.e., the orientation of: the sample itself, the radiation polarization and propagation directions, the static polarization and magnetization directions, and the direction of the toroidal moment related to them. Symbols — experiment, and lines — simulation.

Note that reversing the propagation direction of the radiation is equivalent to reversing the magnetic field, because the magnetoelectric permittivity $\tilde{\alpha}_{xy}$ in Eqn (15) changes sign simultaneously with the field due to the factor $\rho(H)$ in formula (11). Substituting the corresponding dynamic susceptibilities explicitly into Eqn (15), the refractive indices take the following form:

$$n_z^{\pm} \approx \sqrt{\varepsilon_\perp}\left[1+\frac{1}{2}\left(\frac{\Delta\varepsilon_{\rm rot}}{\varepsilon_\perp} \pm 2\eta\sqrt{\Delta\mu_\perp\,\frac{\Delta\varepsilon_{\rm rot}}{\varepsilon_\perp}} + \Delta\mu_\perp\right)L_{\rm F}(\omega)\right], \tag{16}$$

where $\Delta\varepsilon_{\rm rot}(H) = 4\pi\chi^{\rm e}_{\rm rot}(H) = 4\pi\chi^{\rm e}_{0\,\rm rot}/[1+H^2/H_{ab}^2]$, and $\Delta\mu_\perp = 4\pi\chi_\perp$. Expression (16) is valid if the electromagnon contribution to the refractive index is relatively small compared to the lattice contribution $\sqrt{\varepsilon_\perp}$, a condition which is well satisfied for sufficiently large fields, $H \gg H_{ab}$. In the absence of inversion twins ($\eta = \pm 1$), the total electromagnon suppression condition for one of the wave directions reduces to $\Delta\mu_\perp = \Delta\varepsilon_{\rm rot}/\varepsilon_\perp$. However, the electromagnon is not fully suppressed if twins are present, i.e., $|\eta| < 1$.

Turning now to the experimental data, Fig. 7 demonstrates the transmission (panels a, c) and phase shift (panels b, d) spectra for radiation with polarization $\mathbf{h} \parallel a$, $\mathbf{e} \parallel b$ propagating in forward ($k_c > 0$) (panels c, d) and backward ($k_c < 0$) (panels a, b) directions (as noted above, the latter is equivalent to changing the sign of the applied 60- kOe field). It is seen that the electromagnon intensity for the forward propagation (Fig. 7c) is substantially weaker than that for the backward propagation (Fig. 7a), indicating the presence of directional dichroism, a phenomenon in which absorption is different for opposite propagation directions (and which is also observed in some other multiferroics [20–23]). The phase shift spectra normalized to the frequency (optical thickness) also demonstrate that the electromagnon contributes more in the backward (or for $H_b < 0$) (Fig. 7b) than in the forward (Fig. 7d) propagation, indicating the presence of directional birefringence as well. For other polarization ($\mathbf{h} \parallel b$, $\mathbf{e} \parallel a$), no resonance modes were observed — in complete agreement with the analysis above.

In what follows, we will analyze our results using the expression derived for the complex transmission coefficient (amplitude) of a plane-parallel sample for $\mathbf{k} \parallel c$ and for polarization $\mathbf{h} \parallel a$, $\mathbf{e} \parallel b$:

$$t^{\pm} = \frac{(1-r^2)\exp(-{\rm i}k^{\pm}d)}{1-r^2\exp\left[-{\rm i}(k^+ + k^-)d\right]}, \tag{17}$$

where $k^{\pm} = n_z^{\pm}\omega/c$ is the amplitude of the wave vector, $r = (1-z)/(1+z)$ is the reflection coefficient from the sample surface, which is independent of the direction of $\mathbf{k}$, and $z = \sqrt{\tilde{\mu}_{xx}/\tilde{\varepsilon}_{yy}}$, d is the sample thickness. The results calculated for the transmission and the phase shift spectra using virtually the same parameters and shown by solid curves in Fig. 7 agree well with the experimental data.

The relative simplicity of expression (17) for the amplitude of the complex transmission coefficient enables a direct analysis from the experimental transmission and phase shift spectra of the differences in the real, $\mathrm{Re}\,n_z^+ - \mathrm{Re}\,n_z^- = 2\,\mathrm{Re}\,\tilde{\alpha}_{xy}$, and imaginary, $\mathrm{Im}\,n_z^+ - \mathrm{Im}\,n_z^- = 2\,\mathrm{Im}\,\tilde{\alpha}_{xy}$, parts of the refractive indices for the forward and backward propagation directions and thus obtaining the corresponding directional birefringence and dichroism spectra; these are shown in Fig. 8 together with the numerical simulations, which agree well with the experimental data.

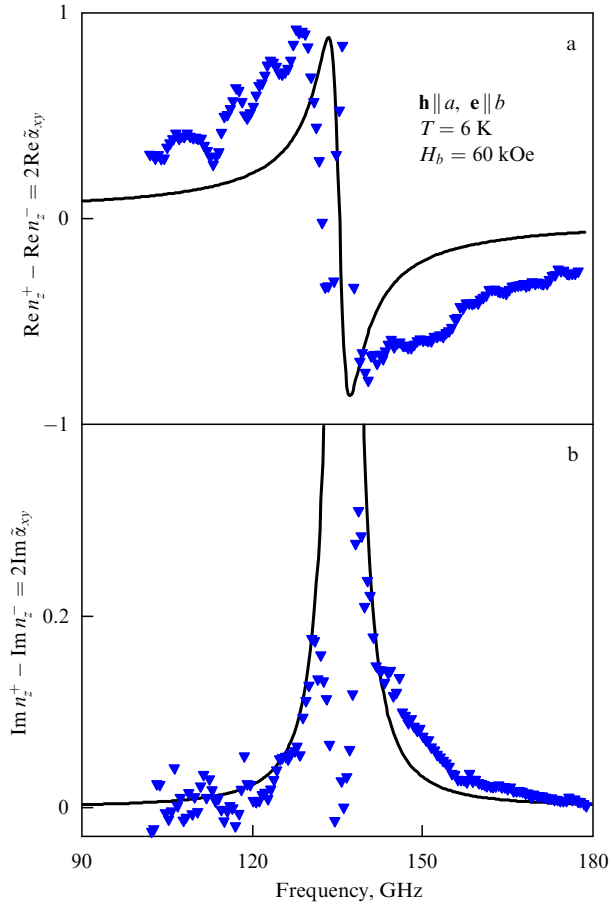

Figure 8. Directional birefringence and dichroism spectra of $SmFe_3(BO_3)_4$ at $H = 60$ kOe close to the electromagnon ($\mathbf{h} \parallel a$, $\mathbf{e} \parallel b$), as determined by the differences in the real and imaginary parts of the refractive indices for the forward and backward radiation propagation directions. The experimental data were obtained from the corresponding transmission and phase shift spectra shown in Fig. 7 and using expression (17). Symbols — experiment, and lines — simulation.

It should be noted that the system in which we observed directional birefringence and dichroism was a twinned sample of $SmFe_3(BO_3)_4$, where these effects cannot fully manifest themselves. In particular, no full mode suppression occurs for one of the propagation directions. Our recent studies [36] on a virtually twin-free substituted compound of $Sm_{0.5}La_{0.5}Fe_3(BO_3)_4$ have demonstrated such an electromagnon suppression close to 100%.

4. Conclusions

The reported gigahertz quasioptical studies on the multiferroic $SmFe_3(BO_3)_4$ showed that rare-earth ferroborates exhibit a low-frequency electroactive AFMR mode (electromagnon), an excitation which has a linear-in-field resonance frequency, contributes dominantly to the giant magnetodielectric effect in $SmFe_3(BO_3)_4$ at low frequencies, and gives rise to the following two electrodynamic effects of magnetoelectric origin:

(a) giant optical activity for $\mathbf{H} \parallel a$, associated with the rotation of the polarization plane of radiation (more than 70 deg mm^{-1} at resonance at 135 GHz and $H = 60$ kOe), and

(b) directional birefringence and dichroism in a transverse magnetic field $\mathbf{H} \| b$, due to asymmetry between radiation propagation in the forward ($\mathbf{k} \| c$) and backward ($\mathbf{k} \| -c$) directions, which is equivalent to changing the sign of the field: $H_b \rightarrow -H_b$.

By taking into account different symmetries of dynamic magnetic responses (magnetic, magnetoelectric, and dielectric susceptibility tensors) for $\mathbf{H} \| a$ and $\mathbf{H} \| b$, a theory was developed which explains and describes quantitatively the observed dynamic magnetoelectric effects and static (quasi-static) properties of $SmFe_3(BO_3)_4$.

Acknowledgments

This work was partially supported by the Russian Foundation for Basic Research (project Nos 14-02-91000, 15-02-07647) and the Austrian Science Funds (I815-N16, I1648-N27, W1243).

References

1. Fiebig M *J. Phys. D Appl. Phys.* **38** R123 (2005)
2. Khomskii D I *J. Magn. Magn. Mater.* **306** 1 (2006)
3. Eerenstein W, Mathur N D, Scott J F *Nature* **442** 759 (2006)
4. Tokura Y *Science* **312** 1481 (2006)
5. Ramesh R, Spaldin N A *Nature Mater.* **6** 21 (2007)
6. Cheong S-W, Mostovoy M *Nature Mater.* **6** 13 (2007)
7. Pyatakov A P, Zvezdin A K *Phys. Usp.* **55** 557 (2012); *Usp. Fiz. Nauk* **182** 593 (2012)
8. Pimenov A et al. *Nature Phys.* **2** 97 (2006)
9. Sushkov A B et al. *Phys. Rev. Lett.* **98** 027202 (2007)
10. Aguilar R V et al. *Phys. Rev. B* **76** 060404(R) (2007)
11. Pimenov A et al. *Phys. Rev. B* **77** 014438 (2008)
12. Mukhin A A et al. *Bull. Russ. Acad. Sci. Phys.* **71** 1617 (2007); *Izv. Ross. Akad. Nauk Ser. Fiz.* **71** 1658 (2007)
13. Kida N et al. *Phys. Rev. B* **78** 104414 (2008)
14. Senff D et al. *Phys. Rev. Lett.* **98** 137206 (2007)
15. Senff D et al. *J. Phys. Condens. Matter* **20** 434212 (2008)
16. Pimenov A, Shuvaev A M, Mukhin A A, Loidl A *J. Phys. Condens. Matter* **20** 434209 (2008)
17. Takahashi Y et al. *Phys. Rev. Lett.* **101** 187201 (2008)
18. Aguilar R V et al. *Phys. Rev. Lett.* **102** 047203 (2009)
19. Mukhin A A et al. *Phys. Usp.* **52** 851 (2009); *Usp. Fiz. Nauk* **179** 904 (2009)
20. Kézsmárki I et al. *Phys. Rev. Lett.* **106** 057403 (2011)
21. Takahashi Y et al. *Nature Phys.* **8** 121 (2012)
22. Takahashi Y, Yamasaki Y, Tokura Y *Phys. Rev. Lett.* **111** 037204 (2013)
23. Kézsmárki I et al. *Nature Commun.* **5** 3203 (2014)
24. Arima T *J. Phys. Condens. Matter* **20** 434211 (2008)
25. Kibayashi S et al. *Nature Commun.* **5** 4583 (2014)
26. Shuvaev A et al. *Phys. Rev. Lett.* **111** 227201 (2013)
27. Zvezdin A K et al. *JETP Lett.* **81** 272 (2005); *Pis'ma Zh. Eksp. Teor. Fiz.* **81** 335 (2005)
28. Zvezdin A K et al. *JETP Lett.* **83** 509 (2006); *Pis'ma Zh. Eksp. Teor. Fiz.* **83** 600 (2006)
29. Yen F et al. *Phys. Rev. B* **73** 054435 (2006)
30. Liang K-C et al. *Phys. Rev. B* **83** 180417(R) (2011)
31. Mukhin A A et al. *JETP Lett.* **93** 275 (2011); *Pis'ma Zh. Eksp. Teor. Fiz.* **93** 305 (2011)
32. Kuz'menko A M et al. *JETP Lett.* **94** 294 (2011); *Pis'ma Zh. Eksp. Teor. Fiz.* **94** 318 (2011)
33. Kuzmenko A M et al. *Phys. Rev. B* **89** 174407 (2014)
34. Volkov A A et al. *Infrared Phys.* **25** 369 (1985); Kozlov G, Volkov A, in *Millimeter and Submillimeter Wave Spectroscopy of Solids* (Ed. G Grüner) (Berlin: Springer, 1998) p. 51
35. Berreman D W *J. Opt. Soc. Am.* **62** 502 (1972)
36. Kuzmenko A M et al. *Phys. Rev. B* **92** 184409 (2015); arXiv: 1505.07813